Near-Intrinsic Energy Resolution for 30 to 662 keV Gamma Rays in a High Pressure Xenon Electroluminescent TPC

V. Álvarez[a], F.I.G.M. Borges[b], S. Cárcel[a], J. Castel[c], J.M. Catalá[d], S. Cebrián[c], A. Cervera[a], C.A.N. Conde[b], T. Dafni[c], T.H.V.T. Dias[b], J. Díaz[a], M. Egorov[e], R. Esteve[d], P. Evtoukhovitch[f], L.M.P. Fernandes[b], P. Ferrario[a], A.L. Ferreira[1], E. Ferrer-Ribas[h], E.D.C. Freitas[b], V.M. Gehman[e], A. Gil[a], I. Giomataris[h], A. Goldschmidt[e,*], H. Gómez[c], J.J. Gómez-Cadenas[a], K. González[a], D.González-Díaz[c], R.M. Gutiérrez[i], J. Hauptman[j], J.A. Hernando Morata[k], D.C. Herrera[c], V. Herrero[d], F.J. Iguaz[c], I.G. Irastorza[c], V. Kalinnikov[f], L. Labarga[l], I. Liubarsky[a], J.A.M. Lopes[b], D. Lorca[a], M. Losada[i], G. Luzón[c], A. Marí[d], J. Martín-Albo[a], A. Martínez[a], T. Miller[e], A. Moiseenko[f], F. Monrabal[a], C.M.B. Monteiro[b], J.M. Monzó[d], F.J. Mora[d], L.M. Moutinho[g], J. Muñoz Vidal[a], H. Natal da Luz[b], G. Navarro[i], M. Nebot[a], D. Nygren[e], C.A.B. Oliveira[e,g], R. Palma[m], J. Pérez[n], J.L. Pérez Aparicio[m], J. Renner[e], L. Ripoll[o], A. Rodríguez[c], J. Rodríguez[a], F.P. Santos[b], J.M.F. dos Santos[b], L. Segui[c], L. Serra[a], D. Shuman[e], A. Simón[a], C. Sofka[p], M. Sorel[a], J.F. Toledo[d], A. Tomás[c], J. Torrent[o], Z. Tsamalaidze[f], D. Vázquez[k], E. Velicheva[f], J.F.C.A. Veloso[g], J.A. Villar[c], R.C. Webb[p], T. Weber[e], J. White[p], N. Yahlali[a]

[a]*Instituto de Física Corpuscular (IFIC), CSIC & Universitat de València, Calle Catedrático José Beltrán, 2, 46980 Paterna, Valencia, Spain*
[b]*Departamento de Fisica, Universidade de Coimbra, Rua Larga, 3004-516 Coimbra, Portugal*
[c]*Laboratorio de Física Nuclear y Astropartículas, Universidad de Zaragoza, Calle Pedro Cerbuna 12, 50009 Zaragoza, Spain*
[d]*Instituto de Instrumentación para Imagen Molecular (I3M), Universitat Politècnica de València, Camino de Vera, s/n, Edificio 8B, 46022 Valencia, Spain*
[e]*Lawrence Berkeley National Laboratory (LBNL), 1 Cyclotron Road, Berkeley, California 94720, USA*
[f]*Joint Institute for Nuclear Research (JINR), Joliot-Curie 6, 141980 Dubna, Russia*
[g]*Institute of Nanostructures, Nanomodelling and Nanofabrication (i3N), Universidade de*

[*]Corresponding author
Email address: agoldschmidt@lbl.gov (A. Goldschmidt)

Aveiro, Campus de Santiago, 3810-193 Aveiro, Portugal
[h]IRFU, Centre d'Études Nucléaires de Saclay (CEA-Saclay), 91191 Gif-sur-Yvette, France
[i]Centro de Investigaciones en Ciencias Básicas y Aplicadas, Universidad Antonio Nariño, Carretera 3 este No. 47A-15, Bogotá, Colombia
[j]Department of Physics and Astronomy, Iowa State University, 12 Physics Hall, Ames, Iowa 50011-3160, USA
[k]Instituto Gallego de Física de Altas Energías (IGFAE), Univ. de Santiago de Compostela, Campus sur, Rúa Xosé María Suárez Núñez, s/n, 15782 Santiago de Compostela, Spain
[l]Departamento de Física Teórica, Universidad Autónoma de Madrid, Campus de Cantoblanco, 28049 Madrid, Spain
[m]Dpto. de Mecánica de Medios Continuos y Teoría de Estructuras, Univ. Politècnica de València, Camino de Vera, s/n, 46071 Valencia, Spain
[n]Instituto de Física Teórica (IFT), UAM/CSIC, Campus de Cantoblanco, 28049 Madrid, Spain
[o]Escola Politècnica Superior, Universitat de Girona, Av. Montilivi, s/n, 17071 Girona, Spain
[p]Department of Physics and Astronomy, Texas A&M University, College Station, Texas 77843-4242, USA

Abstract

We present the design, data and results from the NEXT prototype for Double Beta and Dark Matter (NEXT-DBDM) detector, a high-pressure gaseous natural xenon electroluminescent time projection chamber (TPC) that was built at the Lawrence Berkeley National Laboratory. It is a prototype of the planned NEXT-100 ^{136}Xe neutrino-less double beta decay ($0\nu\beta\beta$) experiment with the main objectives of demonstrating the near-intrinsic energy resolution at energies up to 662 keV and of optimizing the NEXT-100 detector design and operating parameters. Energy resolutions of ∼1% FWHM for 662 keV gamma rays were obtained at 10 and 15 atmospheres and ∼5% FWHM for 30 keV xenon x-rays. These results demonstrate that 0.5% FWHM resolutions for the 2,448 keV hypothetical neutrino-less double beta decay peak are

realizable. This energy resolution is a factor 6 to 20 better than that of the current leading $0\nu\beta\beta$ experiments using xenon in the liquid phase and thus represents a significant advancement.

Keywords: Xenon, HPXe, Energy Resolution, High-Pressure, TPC, Electroluminescence, Double Beta Decay, Neutrinoless, 136Xe, Fano

---

1. Introduction

Neutrino-less double beta decay ($0\nu\beta\beta$) is a postulated[1] rare process in which a nucleus changes by two units of charge while emitting two electrons (or positrons) but without the emission of neutrinos. Should this decay happen in nature the sum of the energies of the two electrons is expected to be monoenergetic at exactly the Q-value of the nuclear decay ($Q_{\beta\beta}$, equal to the mass difference between the parent and daughter nuclei). A precise energy measurement can therefore greatly aid in the identification of the $0\nu\beta\beta$ process in the presence of other more common processes that produce either continuous energy deposition spectra or peaks at well known and well separated energies. The occurrence of $0\nu\beta\beta$ would imply that neutrinos are their own anti-particle[**?**], or Majorana particles. Should neutrinos prove to be Majorana particles the observed prevalence of matter over anti-matter in our universe could be explained through the Leptogenesis mechanism[**?**].

The ^{136}Xe isotope is one of the candidate nuclei in which $0\nu\beta\beta$, in this case $^{136}\text{Xe} \rightarrow {}^{136}\text{Ba} + e^{-} + e^{-}$, could be detectable because the single beta decay which would otherwise dominate the experimental count rate is energetically forbidden. Two currently running experiments are searching for this rare process in ^{136}Xe. EXO [**?**] uses 200 kg of the enriched isotope in a cryogenic liquid xenon Time Projection Chamber[?] (TPC) and KamLAND-Zen [?] uses 330 kg of the isotope dissolved in 1,000 tons of organic scintillator. The energy resolutions for these two experiments are 3-4% and 10% FWHM respectively at the 2.458 MeV[?] $Q_{\beta\beta}$ of the ^{136}Xe decay. It is well known, on the other hand, that xenon in gaseous phase can offer significantly better energy resolution[2] due to its small Fano factor[?] F=0.14 (a measure of the level of fluctuations in the number of ionization electrons). For a xenon gas pressure of less than 40 atm the intrinsic energy resolution is expected to be about 0.3% FWHM near the $Q_{\beta\beta}$. It is thus clear that a xenon detector at moderately high pressure would represent a significant advantage for the search of the $0\nu\beta\beta$ spectrum peak as long as its implementation can preserve a near-intrinsic energy resolution.

NEXT-100 is an experiment[?] that is being constructed to search for $0\nu\beta\beta$ using 100-150 kg of ^{136}Xe in a 10-15 atm TPC at the Canfranc underground laboratory (LSC) under the Pyrenees mountains in Spain. In the TPC, electrons liberated through ionization by the passage of energetic charged particles (such as the two electrons from the $0\nu\beta\beta$ decay) will drift under the presence of a weak electric field towards a small region with a high electric field. The E/P (electric field divided by pressure) in this high field region is such that electrons can gather enough energy to excite xenon atoms, but not enough to ionize them. Most of the excitation energy is ultimately released in the form of ultra-violet (UV) photons of wavelengths near 170 nm and constitutes the electroluminescence (EL)[?] signal. For each ionization electron thousands of EL photons can be produced. An array of photomultiplier tubes (PMTs) then detects a fraction of the UV photons to render a measurement of the total energy released in the gas with a statistical precision near the Fano limit.

The NEXT-100 TPC will provide, in addition to a very precise energy measurement, a 3-D image of the ionization tracks by means of a dense array of silicon photomultipliers[**?**] (SiPMs or MPPCs) installed near the electroluminescence region. This topological information is useful to distinguish between events with 2 electrons emerging from a single point, such as in $0\nu\beta\beta$, from the electrons that result from interactions of gamma rays from natural radioactivty in detector and surrounding materials.

In this paper we present the design, data and results from the NEXT-DBDM (NEXT prototype for Double Beta and Dark Matter) detector, a 1 kg natural xenon electroluminscent TPC that was built at the Lawrence Berkeley National Laboratory. It is a prototype of the NEXT-100 detector with the main objectives of demonstrating the near intrinsic energy resolution at energies up to 662 keV and of optimizing the NEXT-100 detector design, construction, and operating parameters.

2. High Pressure Xenon Electroluminescent TPC

The basic building blocks of the NEXT-DBDM xenon electroluminescent TPC are: a stainless steel pressure vessel, a gas system that recirculates and purifies the xenon at 10-15 atm, hexagonal meshes that establish high-voltage equipotential planes in the boundaries of the drift and the EL region, field cages with hexagonal cross sections to establish uniform electric fields in those regions, an hexagonal pattern array of UV sensitive PMTs inside the pressure vessel and an associated readout electronics and data aquisition

(DAQ) system.

When ionizing radiation traverses the drift region of the TPC, xenon atoms are ionized or excited. Most of the excitation energy is promptly released as a fast scintillation pulse of 172 nm UV photons that lasts 10-30 ns[?]. A fraction of these photons are detected in the PMT array, forming the S1 signal that provides the start time t_0 for the TPC. The ionization (or secondary) electrons, on the other hand, drift for a maximum distance of 8 cm at a velocity of 0.1cm/μs towards the EL region. There they accelerate and produce copious EL UV photons. The same PMT array detects a fraction of these, forming the S2 signal.

In the NEXT-DBDM detector the PMT array and the EL region, which are both hexagonal areas with 12.4 cm between opposite sides, are 13.5 cm away from each other (see Fig.1). Thus point-like isotropic light produced in the EL region illuminates relatively uniformly the PMT array. This geometric configuration also makes the illumination pattern and the total light collection only very midly dependent on the position of the light origin within the EL region. The diffuse reflectivity of the TPC walls increases this light collection uniformity further. As a result, the device provides good energy measurements with little dependence on the position of the charge depositions. On the other hand, without a light sensor array near the EL region as in the current NEXT-DBDM, precise tracking information is not available and only coarse average position can be obtained using the PMT array light pattern.

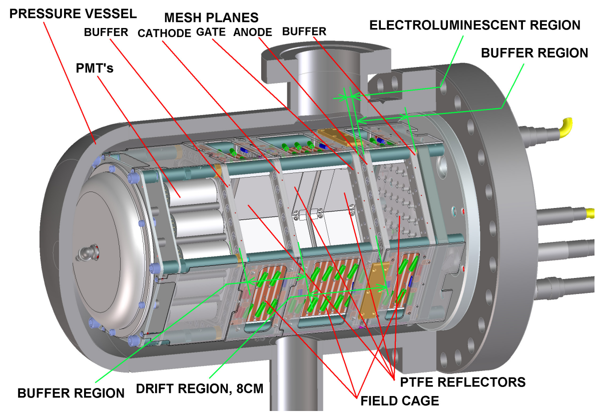

Figure 1: **NEXT-DBDM electroluminescent TPC configuration:** An array of 19 photomultipliers (PMTs) measures S1 primary scintillation light from the 8 cm long drift region and S2 light produced in the 0.5 cm electroluminiscence (EL) region 13.5 cm away from the PMTs. Two 5 cm long buffer regions behind the EL anode mesh and between the PMTs and the cathode mesh grade the high voltages (up to ±17 kV) down to ground potential.

3. Intrinsic Energy Resolution in the HPXe TPC

The intrinsic energy resolution in a xenon gas detector that measures ionization is given by:

$$\delta E/E = 2.35\sqrt{(FW_i/E)}\text{FWHM} \tag{1}$$

where E is the energy released in the detector, W_i is the average energy required to liberate an electron and F is the Fano factor that quantifies the fluctuations in the number of liberated electrons. While F and W_i are energy, drift field and pressure dependent due to electron-ion recombination and due to the energy dependence of the energy loss rate, dE/dx, their values are slowly varying in the range of energies, 30-662 keV, pressures, 10-17 atm, and drift fields, 0.3-2.0 kV/cm, studied here. For the purpose of studying the energy resolution in the NEXT-DBDM detector we used 662 keV gamma rays from a ^{137}Cs source and 28-34 keV xenon x-rays that follow photoelectric interactions of the gamma rays. Thus, for F=0.14 [**?**] and W_i=21.9 eV[**?**] the intrinsic energy resolutions are approximately 0.51% FWHM for 662 keV and 2.3% FWHM for 30 keV.

4. Experimental Aspects of the Energy Resolution in the Electroluminiscent HPXe TPC

4.1. Statistical

In the NEXT-DBDM detector the number of liberated electrons is not measured directly. Rather, those electrons are drifted and then accelerated to produce O(1000) UV photons each of which O(10) are measured as photoelectrons in the PMT array. This gain and measurement sequence introduces fluctuations beyond the intrinsic Fano limit. In Ref.[**?**] a formalism was developed to calculate the energy resolution achievable in light of those additional fluctuations:

$$\delta E/E = 2.35\sqrt{((F+G)W_i/E)}\text{FWHM} \tag{2}$$

with

$$G = 1/\eta + (1+\sigma_{pd}^2)/n_{pe} \tag{3}$$

where η is the average number of UV photons produced in the EL region per secondary electron (or optical gain), n_{pe} is the average number of photons detected (as photoelectrons) per secondary electron and σ_{pd}^2 is the variance on the charge measured for single photoelectrons. In the absence of afterpulsing or noise the charge variance for a typical PMT is $\sigma_{pd}^2 = 0.5$ or less.

The electroluminescence optical gain in pure high pressure xenon is given approximately by[**?**]:

$$\eta = 140\left(\frac{\Delta V}{p\Delta z} - 0.83\right)\cdot p\cdot \Delta z \tag{4}$$

where ΔV is the voltage difference between the electrodes that form the EL region in kilovolts, p is the pressure in atmospheres and Δz is the distance between the electrodes in centimeters. For instance, if p=10 atm, ΔV=11.3 kV and Δz=0.5 cm the EL optical gain is η=1000.

The value of n_{pe} is the product of the EL optical gain η times the collection efficiency (the probability of a UV photon generated in the EL region reaching a PMT window) times the PMT quantum efficiency at the corresponding wavelength. For example for a 10% collection efficiency, a 15% PMT quantum efficiency at the 170 nm of the xenon electroluminescence and η=1000, n_{pe}=15 and the expected energy resolution for 662 keV gamma rays in the absence of systematic effects is 0.66% and 3.11% for 30 keV.

4.2. Systematic

Systematic effects that broaden the energy resolution can be grouped in two categories: position and time dependencies. Position dependencies of the energy response arise, for example, from a non-uniform EL light collection efficiency, a non-uniform EL gain, secondary electron losses due to attachment on electronegative impurites during drift and secondary electrons hitting the TPC walls due to diffusion or due to drift field non-uniformities. Time dependencies of the energy response arise, for example, from time-varying voltages, temperature (and its subsequent effect of gas viscosity, PMT response, etc), gas flow and purity, PMT response and gas density.

In the NEXT-DBDM TPC systematic dependencies of the energy response as a function of the position along the drift (z-axis in our chosen coordinate system) are small due to the high xenon gas purity achieved. In addition, the z position of charge depositions within the drift region is very precisely measured. The opposite is true in the plane perpendicular to the drift direction ($x - y$): the light collection changes more rapidly as a function of distance from the center axis of the TPC and the $x - y$ position of charge depositions is poorly measured. For this reason, to study the energy resolution achievable with the xenon EL TPC, calibration gamma rays are introduced along the center z axis through a narrow aperture collimator. Still, the actual charge depositions happen over an extended region in $x - y$ (and z) due to the length of the electron tracks and due to the multi-site depositions from Compton scatters and from xenon x-rays following photoelctric absorption.

5. Experimental Setup

5.1. Gas System

The main functions of the gas system are to recirculate and purify the xenon at pressures up to 17 atm. A magnetically driven seal-less and oil-less pressure rated (95 atm) pump manufactured by Pumpworks Inc. (model 2070) recirculates the xenon at room temperature at 5-15 standard liter per minute (slpm). For the total system volume of approximately 10 liter at 10 atm pressure the pump recirculates one full volume in about 10 minutes. A pressure rated (18 atm) heated getter from Johnson Matthey (model PureGuard) removes O_2, H_2O, N_2 and many other impurities using a nonevaporable zirconium-based material. The getter operates at a constant 450 degrees Celsius irreversibly removing the impurities through bulk diffusion.

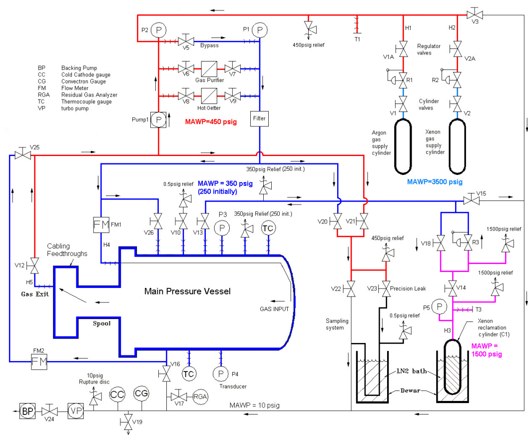

Figure 2: **Gas system schematic (simplified).**

In Figure 2 the complete gas system is shown. Besides the recirculation pump and the heated getter the system includes a vacuum system with a roughing pump (make [illegible]iboVacDry), a turbomolecular pump (make Leybold-Heareus) and Pirani and ion vacuum gauges, a reclamation cylinder where xenon is stored when it is cryogenically removed from the main pressure vessel, an argon purge system, a gas sampling system with a precision leak valve and a residual gas analyzer (model SRS100) and a room temperature secondary getter (SAES model MicroTorr MCP190).

A set of pressure relief valves (with different settings for the various parts of the pressure rated system) and a burst disk in the vacuum system protect the equipment and personel from overpressure hazards.

The typical gas cycle during normal operation of the TPC consists of a vacuum step to 10^{-5} torr, followed by an argon purge and recirculation at 1 atm, a second vacuum step to remove the argon and then the xenon fill from the reclamation cyclinder. After the fill, the recirculation and purification is started and monitored and controlled with gas flow meters (models Sierra Smart-Trak and Omega FM1700) and a variac that powers the recirculation pump to set the recirculation flow.

5.2. Pressure Vessel and Feedthrough Ports

The main pressure vessel **??** is an 8.7 liter stainless steel cylindrical shell of 20 cm diameter and 33.5 cm length with an elliptical head on one end and a custom gasketed Conflat flange (main flange) on the other. Half inch VCR ports on the side of the vessel are used for gas fill, recirculation flow, pressure and temeperature gauges and pressure relief valves. A 5.9 cm diameter (ID) port is used for vacuum pumping. On the main flange there are small ports with commercial high voltage feedthroughs (rated to 20 kV and 17 atm) with additional custom PTFE sleeves on the inside to increase the breakdown voltage when operating with high pressure xenon. A larger central port is used to connect to an octagon-shaped vessel through a long tube with an internal source reentrance tube with a 2mm thick endcap. Signal and high-voltage coaxial cables from the (in-vessel) PMT array pass through the axial extension tube and connect with 32-pin feedthroughs on the side ports of the octagonal vessel.

5.3. TPC

The field configuration in the TPC is established by five stainless steel meshes with 88% open area at 0.5 cm (cathode buffer or PMT mesh), 5.5 cm (cathode or drift start mesh), 13.5 cm (gate or EL-start mesh), 14.0 cm

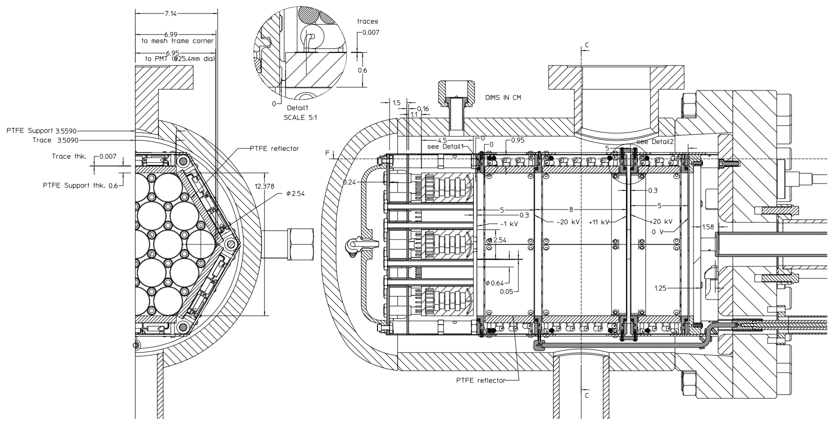

Figure 3: **Cutaway schematic of the TPC.**

(anode or EL-end mesh) and 19.0 cm (anode buffer or ground mesh) from the PMT windows. The meshes are supported and kept tense by stainless steel frames made out of two p[illegible] and [illegible]sioning screws on the perimeter. The TPC side walls, made out of 18 individual rectangular assemblies 7.1 cm wide (and 5 and 8 cm length) connecting adjacent meshes (except around the 0.5 cm EL gap), serve the dual purpose of light cage and field cage. Each side wall assembly is made of a 0.6 cm thick PTFE panel and a ceramic support panel. The FTFE panels are bare on the side facing the active volume and have copper stripes parallel to the mesh planes every 0.6 cm on the other. The bare PTFE serves as reflector for the UV light (a 40-50% Lambertian reflectivity was measured in **??**) to increase the light collection efficiency. Adjacent copper stripes are linked with 100 MΩ resisitors to grade the potential and produce a uniform electric field. The ceramic support panels are connected, mechanically and electrically, to the outer perimeter of the mesh support frames and to the first and last copper stripes on their corresponding PTFE panel. High voltage connections to establish the TPC fields (HHV) are made directly to the mesh frames.

Six short PEEK rods going through holes on the mesh frames' vertices secure the anode and anode buffer meshes to the main vessel flange. Three PEEK c-clamps (on alternate sides of the hexagon) with grooves to prevent HV surface breakdown attach, in turn, the anode mesh to the gate mesh maintaining a gas gap of 0.5 cm. Finally, six PEEK rods support the gate, cathode and cathode buffer meshes as well as the 19-PMT array. Mechanical tolerances obtained are better than 1 mm throughout the TPC geometry.

In the initial implementation of the NEXT-DBDM TPC longer PEEK rods supported the entire assembly going through holes in the anode and gate mesh frames with PEEK spacers to maintain the EL gap. High voltage breakdown in the form of sparks across the gap during HV conditioning and at random times thereafter produced conductive paths on the insulator surface, requiring time consuming repair. The c-clamp solution described above made the TPC completely resilient to the unavoidable occasional sparking.

Clean gas from the purification system flows through an internal tube to an enclosed volume behind the PMTs and reaches the active volume through small dedicated PEEK tubes between the PMTs to exit the TPC through a port on the octagonal vessel at the end of the extension tube.

A wide range of HHV voltages were used to investigate the TPC performance dependence on drift electric field and on the E/P in the EL region:

cathode voltages from -4 to -13 kV, gate voltages from -1 to -10 kV and anode voltages from 1 to 13 kV.

5.4. PMTs, Readout and Data Processing

The PMT array is composed of nineteen 2.54 cm diameter Hamamatsu 7378A PMTs. These PMTs, with fused silica windows, have a quantum efficiency of ∼15% for 170 nm xenon light. The PMTs were individually pressure tested to 19 atm (absolute) and no mechanical or performance failures were observed. The HV, typically about -1000V, is individually set to get a $\sim 10^6$ gain. The bases for the PMT array are implemented in a single hexagonal PCB board with surface mount components and with pin sockets that provide both mechanical support for the PMTs as well as the necessary electrical connections. The base has about 1 MΩ, thus power dissipation is about 1 Watt per PMT, and 1 μF capacitors connected to the last dynode stages to keep the gain constant during long EL light pulses. 200 pF capacitors connected from the PMT anodes to ground slow down the return to the baseline after a pulse so that all photoelectrons are properly sampled in the 100 MHz digitizers.

PMT anode signals travel through ∼1 m long PTFE coaxial cables to the 32-pin feedthoughs and then to 8-channel Phillips-777 amplifiers set to a gain of 40. The amplified signals are then stretched and attenuated in a passive RCR circuit to reduce high frequency noise and to match the input range of the SIS3302 16-bit digitizers that sample the individual PMT signals at 100 mega-samples per second. PMT waveform data, typically 16,384 samples or 163.84 μs, are readout through an SIS3150 USB to VME interface to a Linux server for processing, analysis and storage. The overall system noise is such that individual photoelectrons can be detected and the instantaneous (10 ns) dynamic range per PMT is 1-to-200 photoelectrons. Custom-written DAQ software is used to control the data acquisition.

The trigger is designed to identify S2 EL pulses. It is formed based on a single PMT by a 12μs peaking-time shaping amplifier followed by a discriminator. The trigger is used as a stop signal (with a stop delay) for the digitizers such that there are, typically, 80 μs of waveform data preceeding the first S2 pulse and 80 μs after. Since the maximum drift time is about 80 μs, this permits the search for the S1 pulse in the offline analysis while ensuring that all the S2 light from one event is measured.

After a block of 512 events is collected with about 100 MBytes in raw DAQ data format, an automated process unpacks the data, applies calibration constants to the individual PMTs and executes the analysis code based on ROOT[**?**] and FMWK[**?**] that finds S1 and S2 pulses and computes energies, times and positions and outputs the results in a 1 MBytes ROOT data trees.

5.5. Controls and Monitoring

All system controls (except the single PMT HV power supply), such as HHV voltage settings and current limits and recirculation flow, are done manually. The three HHV voltages and currents, the PMT HV power supply voltage, the pressure inside the TPC vessel, the temperature in two points inside the TPC and the room temperature are automatically and continuously logged for monitoring and to aid in offline data analysis. The recirculation flow is manually logged.

6. Data Analysis

In the first step of the data analysis the individual PMT waveforms are changed to photoelectron units using calibration constants from dedicated low occupancy single photoelectron runs with short LED light pulses. A sum waveform is then computed from a sample-by-sample addition of the 19 PMTs' waveforms and the baseline of the sum waveform is obtained. A search for S1 and S2 pulses that cross a threshold, determined from the value of the baseline noise, follows. Pulses are defined as S1 candidates if they are less than 500 ns wide, all other pulses are considered S2 candidates. Individual pulses are integrated and the largest S1 candidate is assumed to be the event's start time and the others discarded. All S2 pulses that follow the chosen S1 are considered part of the event while the ones preceeding it are discarded. An event is considered valid if it has and S1 pulse with at least one associated S2 pulse. Figures 4 and 5 show typical valid events from 662 keV ^{137}Cs gamma ray interactions.

During the automatic analysis of the data, the electron attachment lifetime of the gas is not yet known. In order to enable the offline correction of these charge losses the ten first moments of the S2 charge distribution $\int q(t)t^n dt$ with n=0,1...,9 are calculated where t is the time interval since the S1 start time pulse.

An average x-y position for the event is calculated from an S2-charge weighted average of the PMT positions. The event is also time split into equal-charge slices. For each slice an average x-y poistion is computed from the PMT light distribution. This provides x-y-z positions for well separated energy depositions such as from Compton scatters or from x-rays following

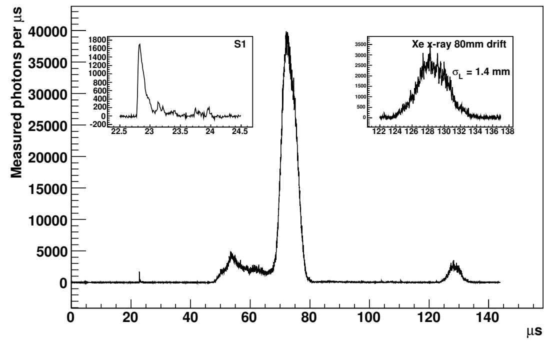

Figure 4: **Typical full energy 662 keV gamma ray event waveform:** the sum of the previously calibrated 19 photomultipliers' waveforms is shown. The S1 pulse (shown in detail in the left inset) due to xenon scintillation is short and with O(200) measured photons. Two S2 pulses caused by electroluminescence of xenon from ionization electrons follow. The first with ∼270,000 measured photons is likely due to a 630 keV electron from the photelectric interaction of the 662 keV gamma ray; the pulse structure reflects the ionization density of the track along its ∼2.5 cm long projection on the drift (z) direction. The second (shown in detail in the right inset) with ∼12,000 measured photons is likely due to the interaction, a few cm away, of a 30 keV xenon x-ray following the photoelectic process; since the 30 keV energy deposition is nearly point-like the pulse shape is gaussian with a σ_L of 1.4 mm set by the longitudinal diffusion of the electrons during the ∼8 cm drift. This event is from a data run taken at 10 atm with a 0.16 kV/cm drift electric field and an E/P of 2.1kV/(cm atm) in the EL region.

photoelectric interactions.

7. Results

7.1. PMT Performance

As shown in formulas 2 and 3 the energy resolution achievable in an electroluminescent TPC depends on the precision with which individual photons

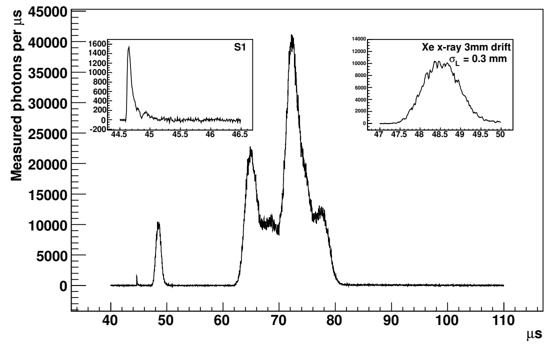

Figure 5: **A second typical full energy event:** In this event from the same data run as in Fig.4 the xenon x-ray interacted close to the EL region and thus the ionization electrons drifted for just 3mm and underwent a correspondingly small longitudinal diffusion σ_L of 0.3 mm.

can be measured. System noise and the variance from the avalanche multiplication in the PMT (mostly from the first dynode stages) contribute to the spread of the charge measured for photoelectrons. It was found, however, that the charge fluctuations due to PMT after-pulsing are the dominant factor in the photoelectron charge resolution. After-pulsing caused by the occasional ionization of residual gas molecules in the PMT vacuum volume can produce delayed pulses with large charges (10-20 photoelectron charges are not uncommon). Dedicated LED data runs with light pulses less than 100 nsec long (first afterpulse peaks from hydrogen and helium ions appear at 200 and 300 nsec for these small PMTs) were thus taken to assess the charge-variance for each PMT. The typical value was found to be $\sigma(Q)/Q = 1.2$ thus σ_{pd}^2=1.44 with small PMT-to-PMT variations.

7.2. Position Measurement

The TPC configuration with the PMT array 13.5 cm from the EL region does not permit detailed track reconstruction in the x-y plane. Still, the position reconstruction achievable allows the fiducialization of pulses to select events/pulses within regions of the TPC with uniform light collection efficiencies. The position reconstruction for isolated 50-100 keV energy depositions shown in Fig. 6 displays the hexagonal boundary of the TPC. A scaling factor of $\sim$30 is needed to convert charge-weighted average x and y positions to true TPC xy coordinates.

Several data runs were taken with LED light pulses of various intensities to determine the position resolution for point depositions of charge as a function of the amount of light produced and detected. Figure 7 shows the obtained position resolutions which approximately follow the expected $1/\sqrt{N}$ dependency on the photon statistics.

7.3. Energy Measurement

The energy measurement is derived from the summed waveform (in photons detected) of all S2 pulses following the event S1 pulse. Figure 8 shows a calibrated spectrum obtained from the ^{137}Cs source collimated with the gamma rays entering the chamber along its central axis. The full energy peak events in this data run have $\sim$270,000 detected photons which, for W_i=21.9 eV, corresponds to about 8.9 photons detected per ionization (secondary) electron. Using the nominal EL gain η=846 from Eq.4 the total number of photons produced is $846 \cdot 662,000/21.9 \simeq$25.5 million. From this, an S2-photon detection efficiency slightly larger than 1% is deduced.

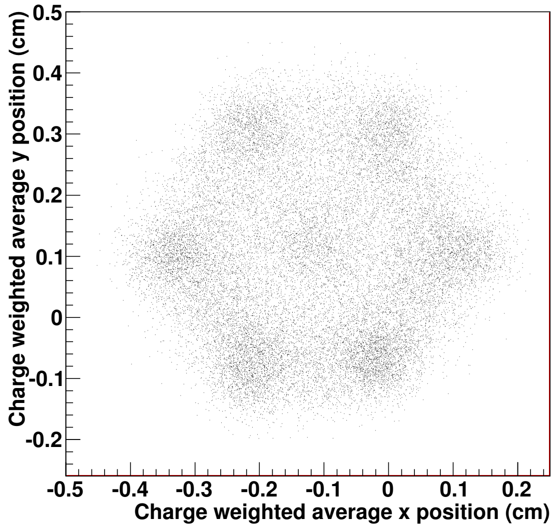

Figure 6: **Position reconstruction:** The charge-weighted average of the 19 PMT positions is used for x-y reconstruction. Events with energy depositions between 50 and 100 keV were selected; at these energies ionization tracks extend for just a few mm and produce enough light to reconstruct with suficient position resolution. The edges of the hexagonal area correspond to the TPC cross section. Due to the spatial uniformity of the PMT plane illumination a scaling of factor of $\sim$30 (not applied here) is needed to obtain true x-y positions from these charge-weighted averages. These data were taken with the ^{137}Cs source, at 10 atm and with E/P of 2kV/(cm atm) in the EL region.

While the spectrum was calibrated only using the 662 keV line, the xenon x-rays peak appears at the correct energy (around 30 keV) confirming the expected linearity of the energy measurement in the interval of interest here.

Attachment losses of drifting secondary electrons can be assessed from the full energy peak position as a function of the drift time of the events. Figure 9 shows typical data for 10 and 15 atm with excellent electron lifetimes of 36 and 9 milliseconds, respectively. Less than 1% of the electrons are lost

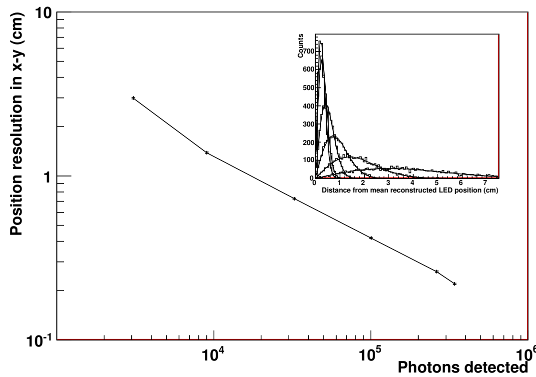

Figure 7: **Position resolution for LED light pulses:** The position resolution in the x-y plane as a function of the number of detected photons is shown. The resolution is derived from data from light pulses from an 378 nm LED located behind the PTFE backplane, which diffuses its light, and illuminates the PMT plane from about 19 cm distance. The inset shows the radial distributions (and fits) from which the individual resolution values were obtained.

to attachment for the maximum 8 cm drift length. Assuming that the main source of electron attachment is due to residual O_2, the measured electron lifetime at 10 atm corresponds to a residual oxygen component at the 2-4 part per billion. The lower lifetime at 15 atm is due to the pressure dependence of the 3-body attachment process rate.

The S2 photon collection efficiency is expected to vary somewhat as a function of the x-y position because of solid angle and chamber optics (wall reflectivities,etc). A sample of xenon x-ray energy depositions was used to measure the change in photon detection efficiency as a function of the radial position. Figure 10 shows this dependence derived from a run in which individual x-rays where reconstructed with $\sim$0.8 cm resolution in x-y. For the purpose of this measurement x-ray depositions can be considered point-

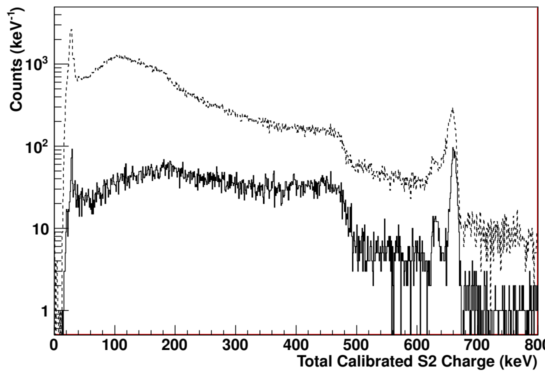

Figure 8: **Energy spectrum for ^{137}Cs 662 keV gamma rays:** The dashed line shows the calibrated spectrum (using the full energy 662 keV peak alone) from a data run taken at 10 atm with a 0.3 kV/cm drift electric field and an E/P of 2 kV/(cm atm) in the EL region. The 1 mCi source is heavily collimated and its gamma rays enter the TPC along the drift axis (z). Below the full energy peak at 662 keV, the smaller x-ray escape peak at ∼630 keV, the Compton edge at 477 keV and the xenon x-ray peak at ∼30 keV can be seen. The solid line is the same spectrum with a requirement that the reconstructed average position of an event be less than ∼1.2 cm form the TPC axis. The small feature near 184 keV is due to Compton backscatters. The no-source background spectrum (not shown) has a broad peak near 100 keV.

like because 30 keV electron tracks at these pressures extend typically for less than half a millimeter. A nearly flat response is seen up to 2 cm radius and then a linear decline in response towards the outer edge of the TPC where the collection is about 10% lower than in the center.

In the absence of detailed track imaging, the radial dependence of the detector response to point-like depositions affects the TPC energy resolution for extended tracks. Electron tracks from 662 keV gamma interactions at the pressures of interest here have 2-4 cm spans and nearly random shapes

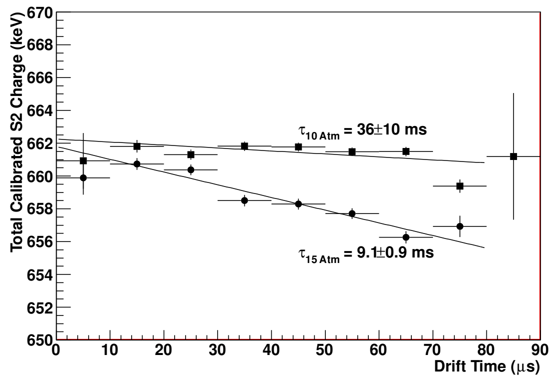

Figure 9: **Electron attachment losses:** The average calibrated S2 charge versus the charge-weighted drift time is shown for full energy events. Attachment lifetimes are obtained from the shown exponential fits. The 10 atm data was taken with a 0.19 kV/cm field in the drift region and the 15 atm data with 0.59kV/cm.

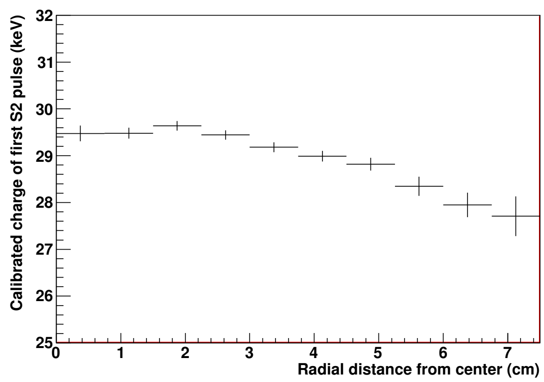

Figure 10: **Radial dependence of energy response:** Xenon x-ray energy depositions were selected from full-energy 662 keV events for which the first S2 pulse has energy in the 20-40 keV range. The reduced response at larger radial positions (also observed in a detailed Monte Carlo simulation of the TPC) is due to geometric and optical effects of the EL light collection efficiency. These data were taken at 10 atm with a 1.0 kV/cm field in the drift region and 2.68 kV/(cm atm) in the EL region.

due to the large coulomb multiple scattering in xenon. Figure 11 shows the effect of a radial cut on the energy resolution of 662 keV depositions and its efficiency. Since the collimated gamma rays enter the chamber along the main axis, events with a small average radial position have better energy resolution primarily because they span a smaller radial range.

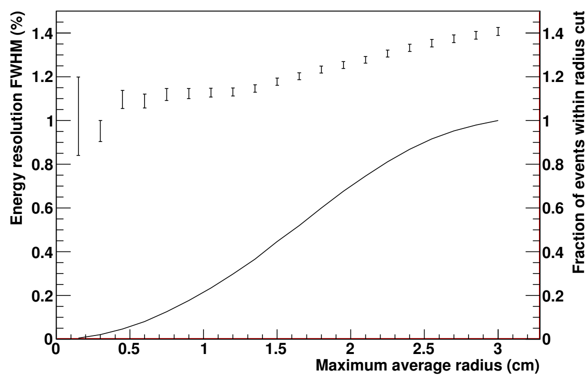

Figure 11: **Energy resolution dependence on radial cut:** Full energy 662 keV events are chosen and, for each, an average x-y position is computed (and scaled to true TPC coordinates) using all of the S2 signal. The FWHM energy resolution (data points) is obtained from a gaussian fit to the peak after placing a cut on the radial position (the abscissa). The radial cut efficiency (solid line and right ordinate axis) is also shown. These data were taken at 10 atm with a 0.16 kV/cm field in the drift region and 2.1 kV/(cm atm) in the EL region.

Figure 12 shows the improvement in the measured energy resolution for 662 keV depositions with increased EL light yield. As seen in Eq. 2 and 3 the G term dominates the resolution at low light yields (n_{pe} small) while the intrinsic Fano term is the asymptotic resolution in the large light yield limit.

In Fig. 13 the energy spectrum in the 662 keV full energy region obtained at 10 atm is shown. A 1.1% FWHM energy resolution was obtained for

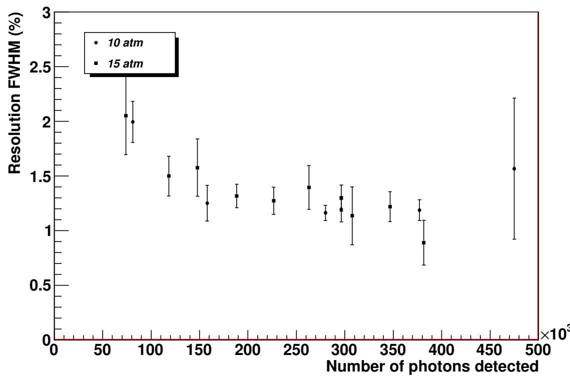

Figure 12: **Energy resolution dependence on amount of light detected:** 662 keV full energy peak resolutions are shown for data runs with different total S2 light yield (controlled primarily by the E/P in the EL region). Energy spectra were obtained by selecting events reconstructed in the central 1 cm radius region and with an S1 signal with more than 100 measured photons and not more than 600. A small electron drift-time-dependent attachment correction is applied. The expected $\sim 1/\sqrt{N}$ improvement is observed. These data were taken with drift fields of 0.5-0.6 kV/cm at 10 atm and 0.16-0.72 kV/cm at 15 atm.

events reconstructed in the central 0.6 cm radius region. A small drift-time dependent correction for attachment losses with $\tau = 13.9$ ms was applied. The xenon x-ray escape peak is clearly visible ~30 keV below the main peak. For the spectrum taken at 15 atmospheres, shown in Fig. 14, a 1% FWHM resolution was obtained. At this higher pressure the xenon x-ray is less likely to escape from the active volume and the escape peak almost disappears. This resolution extrapolates to 0.52% FWHM at $Q_{\beta\beta}$=2.458 MeV if the scaling follows a statistical $1/\sqrt{E}$ dependence.

In order to study the EL TPC energy resolution at lower energies, full energy 662 keV events that had a well separated x-ray pulse reconstructed

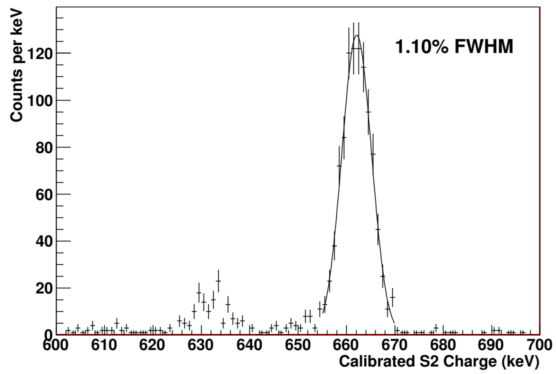

Figure 13: **Energy resolution at 10 atm for 662 keV gamma rays:** These data were taken at 10.1 atm with a 0.16 kV/cm field in the drift region and 2.08 kV/(cm atm) in the EL region. If assumed to follow a $1/\sqrt{N}$ dependence this resolution extrapolates to 0.57% at $Q_{\beta\beta}$=2.458 MeV.

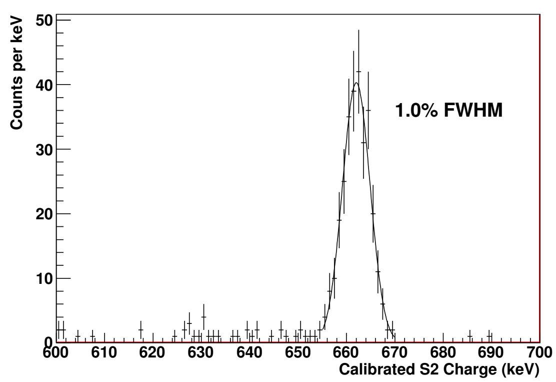

Figure 14: **Energy resolution at 15 atm for 662 keV gamma rays:** A 1.0% FWHM energy resolution was obtained for events reconstructed in the central 0.75 cm radius region. The attachment losses correction with τ = 9.0 ms was applied. A PMT with a clear time varying response was removed from the measurement. These data were taken at 15.1 atm with a 0.59 kV/cm field in the drift region and 1.87 kV/(cm atm) in the EL region.

in the central 1.5 cm radius region were used. The energy calibration was done on the 662 keV full energy peak and linearity with a zero intersect was assumed. Figure 15 shows the energy spectrum obtained at 10 atm with a 5% FWHM resolution. The spectrum was fit to the sum of four gaussians with relative positions and intensities fixed to the strongest xenon x-ray lines [?]. The absolute position of the anchor peak and the peaks' widths (all assumed the same) were obtained from the fit. The anchor peak is at 29.1 keV, less than 2% away from its nominal 29.6 keV value.

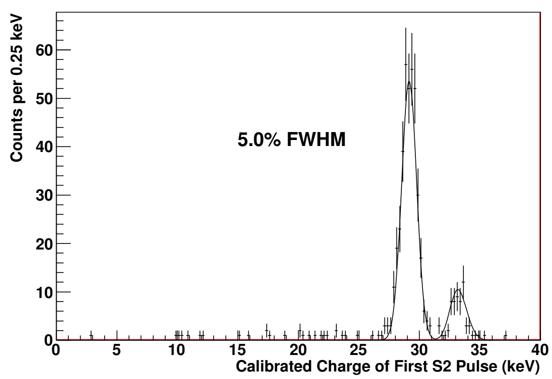

Figure 15: **Energy resolution at 10 atm for 30 keV xenon x-rays:** A 5% FWHM energy resolution for 30 keV was obtained These data were taken at 10.1 atm with a 1.03 kV/cm field in the drift region and 2.68 kV/(cm atm) in the EL region.

Figure 16 summarizes our measurements and understanding of the EL TPC energy resolution. The lower diagonal line represents the Poisson statistical limit from the measurement of a small fraction of the photons produced by the EL gain while the upper diagonal line includes the degradation (mostly from PMT afterpulsing) due to PMT response. The circle data points show the energy resolutions obtained for dedicated LED runs with varying light intensities per LED pulse. The LED points follow the expected resolution over the two decades range studied. The two horizontal lines represent the xenon gas nominal intrinsic resolution for 30 and 662 keV, respectively, and the two curved lines are the expected EL TPC resolutions with contributions from the intrinsic limit and the photons' measurement. Our 662 keV data (squares) and xenon x-ray data (triangles) taken with various EL gains follow the expected functional form of the resolution but are 20-30% larger possibly due to the x-y response non-uniformity. Detailed track imaging from a dense photosensor array near the EL region, such as the one being currently commissioned for the NEXT-DBDM prototype, will enable the application of x-y position corrections to further improve the energy measurement.

In Ref. citeBolotnikov, a study of the energy resolution for 662 keV gamma rays at pressures near condensation (30 atm and above) using a xenon ionization chamber found an improvement of the resolution for increased drift fields. Asymptotic optimum resolutions were achieved only after applying 4 kV/cm or larger fields. Since these large fields would be difficult to achieve in a detector with one meter long drift region such as the one planned for NEXT-100, we investigated the resolution dependence on the drift electric field at 10 atm. Figure 17 shows no discernible dependence in the 0.16-1.03 kV/cm region investigated.

7.4. EL TPC characterization: light yield, drift velocity and longitudinal diffusion

While the study of the energy resolution achievable in the EL TPC was the main goal of this work, we pursued other measurements as well as cross checks against previous results by others. Figure 18 shows the linearity of

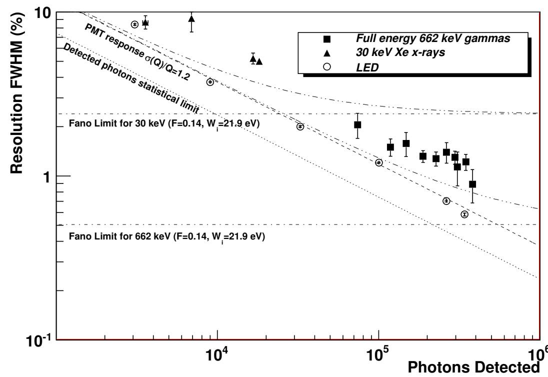

Figure 16: **Energy resolution in the high-pressure xenon NEXT-DBDM electroluminescent TPC:** Data points show the measured energy resolution for 662 keV gammas (squares), ~30 keV xenon xrays (triangles) and LED light pulses (circles) as a function of the number of photons detected. The expected resolution including the intrinsic Fano factor, the statistical fluctuations in the number of detected photons and the PMT charge measurement variance is shown for x-rays (dot dot dashed) and for 662 keV gammas (dot dot dot dashed). Resolutions for the 662 keV peak were obtained from 15.1 atm data runs while x-ray resolutions we obtained from 10.1 atm runs.

the EL light yield as the E/P in the 0.5 cm EL region is varied from 1 to 2 kV/(cm atm) at 15 atmospheres and from 1 to 3 kV/(cm atm) at 10 atmospheres. At these pressures xenon deviates from the ideal gas behavior at the 10% level. Therefore, the more appropriate variables to describe the process are density (N) and reduced electric field (E/N). Figure 19 shows the density normalized EL yield as a function of the reduced field. As expected, points from the 10 and 15 atm data sets follow the same linear trend with consistent slope and threshold.

The electron drift velocity was obtained from the maximum drift times measured (which correspond to the full drift length of 8 cm) for x-ray energy

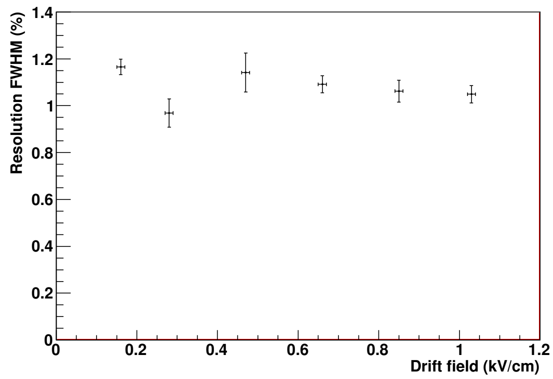

Figure 17: **Energy resolution dependence on drift field:** These data were taken at 10.1 atm with 2.1 - 2.7 kV/(cm atm) in the EL region. The energy resolution attained is largely independent of the drift electric field in the investigated range.

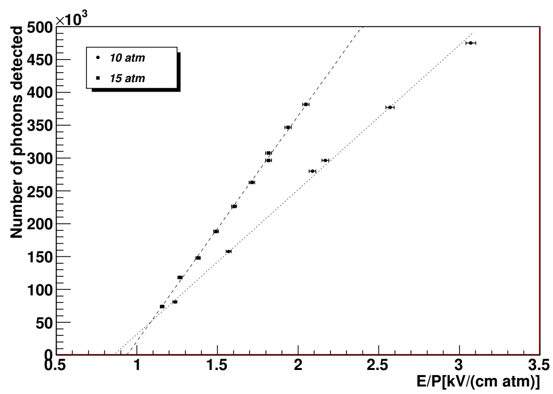

Figure 18: **Light yield dependence as a function of E/P in the EL region**

depositions. Figure 20 shows the drift velocity measured for various drift fields along with two Monte Carlo calculations **????** using up-to-date xenon-electron collision cross sections. While the data points follow the trend in the calculations, 10% deviations are seen at the lower drift fields. Yet, the general agreement observed validates the pressure and field measurements as

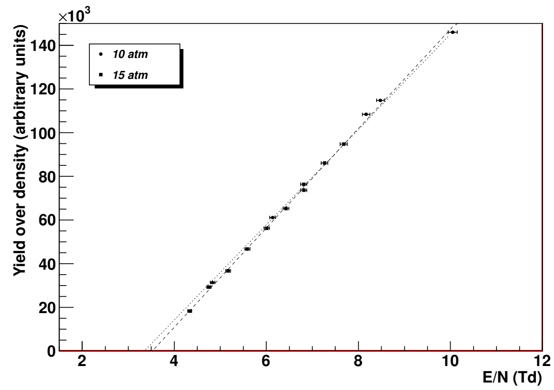

Figure 19: **Density normalized light yield vs. EL reduced field.**

well as the drift field uniformity and the xenon purity.

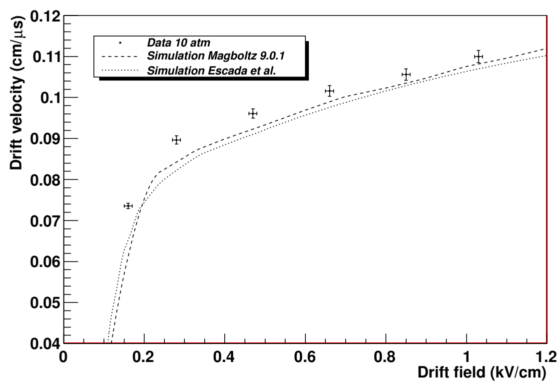

Figure 20: **Drift velocity dependence on drift field:** These data were taken at 10.1 atm.

The longitudinal diffusion was calculated from the time spread of EL light of x-ray depositions (see example fits in the upper right insets of Figs. 4 and 5) and using the measured drift velocity. For x-ray pulses with long drift times the longitudinal diffusion is the dominant source of pulse width with subdominant contributions from the transit time of electrons through the EL gap and from the ionization track length. Figure 21 shows the dependence of the logitudinal diffusion on the drift field and the corresponding Monte Carlo calculations that mostly bracket the data.

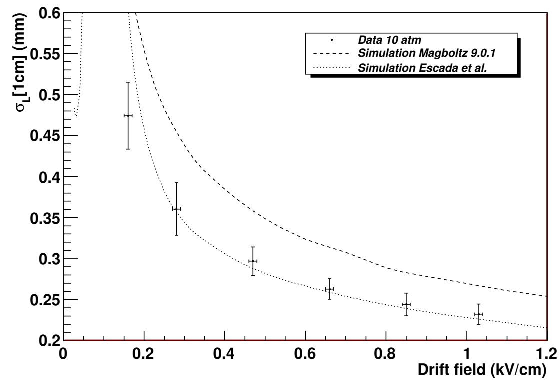

Figure 21: **Longitudinal diffusion dependence on drift field:** The measured longitudinal diffusion is presented here as the σ spread along the drift direction for a 1 cm drift. These data were taken at 10.1 atm.

7.5. S1 measurement

Unlike the S2 light which is generated within a small 0.5 cm region in z, the S1 photons are produced throughout the entire TPC volume wherever the primary ionization happened. As a result the S1 charge (number of photons detected) shows large event-by-event variations. S1 light collection efficiency is largest for events closer to the PMT array due to the larger solid angle. Figure 22 shows the S1 signal's dependency on the average z position of the event. Between 0.2 and 0.45 S1 photons are detected per keV of energy deposited. This S1 yield is consistent with the known W_s, the average energy loss required to liberate one primary scintillation photon in gaseous xenon[**?**], and the photon collection and detection efficiency in our TPC. S1 photons are produced from direct excitations of xenon atoms by the ionizing particle and by ion-electron recombinations. The latter component is, in general, field and pressure dependent. Figure 22 shows less than 10% differences between the S1 yield of runs taken with reduced fields of 0.04 and 0.10 kV/(cm atm) in the drift region.

8. Comparison with Expectations and Simulations?

Compare with resolution formula?

Compare spectra with MC?

Compare Position distributions with MC?

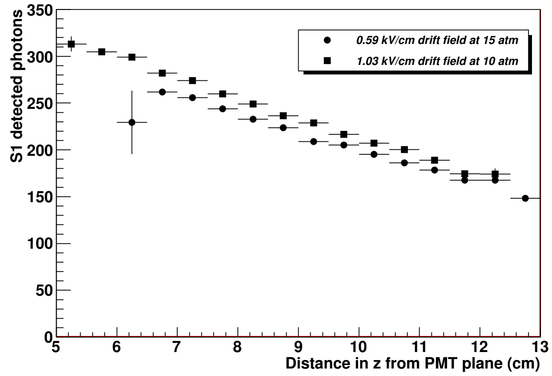

Figure 22: **S1 signal dependence on z position:** For events with full energy 662 keV depositions, the number of measured S1 photons is shown versus the average distance of the ionization track from the PMT plane (obtained from the S2 charge-weighted drift time and the measured drift velocity). The Two runs are shown with E/P in the drift region of 0.04 and 0.10 kV/(cm atm) with very similar S1 yield.

9. Future Developments and Plans

10. Conclusions

11. Acknowledgements

NERSC, KA15, NS?

[1] E. Majorana, Theory of the Symmetry of Electrons and Positrons, Nuovo Cim. 14 (1937) 171–184. doi:10.1007/BF02961314.

[2] A. Bolotnikov, B. Ramsey, The spectroscopic properties of high-pressure xenon, Nucl. Instr. and Meth. A 396 (3) (1997) 360 – 370. doi:10.1016/S0168-9002(97)00784-5.